Binding of Ferric Heme by the Recombinant Globin from the Cyanobacterium *Synechocystis* sp. PCC 6803[†]

Juliette T. J. Lecomte,* Nancy L. Scott, B. Christie Vu, and Christopher J. Falzone

Department of Chemistry and Center for Biomolecular Structure and Function, The Pennsylvania State University, University Park, Pennsylvania 16802

Received February 2, 2001; Revised Manuscript Received March 23, 2001

ABSTRACT: The product of the cyanobacterium *Synechocystis* sp. PCC 6803 gene slr2097 is a 123 amino acid polypeptide chain belonging to the truncated hemoglobin family. Recombinant, ferric heme-reconstituted *Synechocystis* sp. PCC 6803 hemoglobin is a low-spin complex whose endogenous hexacoordination gives rise to optical and NMR characteristics reminiscent of cytochrome b_5 [Scott, N. L., and Lecomte, J. T. J. (2000) *Protein Sci. 9*, 587−597]. In this work, the sequential assignments using $^{15}N-^{13}C$-labeled protein, ^1H nuclear Overhauser effects, and longitudinal relaxation data identified His70 as the proximal histidine and His46 as the sixth ligand to the iron ion. It was also found that one of two possible heme orientations within the protein matrix is highly preferred (>90%) and that this orientation is the same as in vertebrate myoglobins. The rate constant for the 180° rotation of the heme within a protein cage to produce the favored isomer was 0.5 h^{-1} at 25 °C, approximately 35 times faster than in sperm whale myoglobin. Variable temperature studies revealed an activation energy of 132 ± 4 kJ mol^{-1}, similar to the value in metaquomyoglobin at the same pH. The rate constant for heme loss from the major isomer was estimated to be 0.01 h^{-1} by optical spectroscopy, close to the value for myoglobin and decades slower than in the related *Nostoc commune* cyanoglobin. The slow heme loss was attributed in part to the additional coordination bond to His46, whereas the relatively fast rate of heme reorientation suggested that this bond was weaker than the proximal His70−Fe bond. The standard reduction potential of the hexacoordinated protein was measured with and without poly-L-lysine as a mediator and found to be ∼−150 mV vs SHE, indicating a stabilization of the ferric state compared to most hemoglobins and b_5 cytochromes.

Among recently discovered representatives of invertebrate globins are several proteins with a sequence abbreviated by 30−40 residues. These "truncated hemoglobins" (trHb's)[1] are found in the eukaryotic genera *Chlamydomonas* (*1*), *Tetrahymena* (*2*), and *Paramecium* (*3*) and in an increasing number of bacteria. As a group, trHb's vary considerably in primary structure (Figure 1), some displaying pairwise amino acid identity below 30%. The function of most of these proteins is not entirely understood, but it appears that they can perform various roles including the scavenging of oxygen (*4*), its delivery (*5*), its sensing (*6*), and the processing of NO (*7*). Extensive characterization of wild-type and artificially modified vertebrate globins has revealed robust trends in the relationships between structure and reactivity (*8*−*10*). However, the differences between truncated and full-length sequences are too many for these vertebrate trends to apply, and the subset of trHb's requires its own systematic studies to expose functional determinants.

The X-ray structures of the eukaryotic *Chlamydomonas eugametos* and *Paramecium caudatum* trHb's are now available (*11*) and provide useful working models for other trHbs. Figure 2A presents the backbone trace of *C. eugametos* trHb and shows how the shorter fold differs from that of the canonical β globin. The β globin fold contains eight helices, called A through H, arranged in a unique three-on-three helical sandwich. The B, G, and H helices define one face of the molecule and the A, E, and F helices, the other. In *C. eugametos* and *P. caudatum* trHb, the A helix is reduced to a single turn. Most of the CD corner and D helix are missing, and the B and E helical axes have rotated with respect to the other helices. The one-turn F helix is preceded and followed by large loops, referred to as EF and FG. Remarkably, these alterations transform the three-on-three fold into a two-on-two fold (B−E/G−H) unprecedented in globins.

The changes in structure imposed by the shorter sequence are accompanied by changes in the heme−protein contacts.

[†] This work was supported in part by National Institutes of Health Grant GM-54217 and in part by National Science Foundation Grant MCB-91182.

* To whom correspondence should be addressed at the Department of Chemistry, The Pennsylvania State University, 152 Davey Laboratory, University Park, PA 16802. Telephone: (814) 863-1153. Telefax: (814) 863-8403. E-mail: jtl1@psu.edu.

[1] Abbreviations: 1D, one dimensional; 2Q, two quantum; 2QF-COSY, double-quantum-filtered correlated spectroscopy; CD, circular dichroism; dd, distilled deionized; DSS, 2,2-dimethyl-2-silapentane-5-sulfonate; EDTA, ethylenediaminetetraacetic acid; FID, free induction decay; GlbN, cyanoglobin; Hb, hemoglobin; HSQC, heteronuclear single-quantum coherence; IEF, isoelectric focusing; MALDI, matrix-assisted laser desorption ionization; Mb, myoglobin; MRE, molar residual ellipticipty; NOE, nuclear Overhauser effect; NOESY, two-dimensional nuclear Overhauser effect spectroscopy; OSWV, Osteryoung square-wave voltammetry; p*I*, isoelectric point; ppm, parts per million; rHb, recombinant hemoglobin; SHE, standard hydrogen electrode; TOCSY, totally correlated two-dimensional spectroscopy; TPPI, time-proportional phase incrementation; trHb, truncated hemoglobin; Tris, tris(hydroxymethyl)aminomethane; WATERGATE, water suppression by gradient-tailored excitation; WEFT, water-eliminated Fourier transform.

10.1021/bi010226u CCC: $20.00
Published on Web 05/04/2001

```
                          AAAAAAAAAAAAAAAA   BBBBBBBBBBBBBBBBCCCCCCC        DDDDDDDEEEEEEEEEEEEEE
                          1234567891111111   12345678911111111234567        12345671234567891111 1
                                   0123456           0123456                              012345
MYOGLOBIN  : ----------VLSEGEWQLVLHVWAKVEA--DVAGHGQDILIRLFKSHPETLEKFDRFKHLKTEAEMKASEDLKKHGVTVLTAL
                               1        1         2         3                    4         5
                                        0         0         0                    0         0
SYNECHOCYST: -------------------MSTLYEKLGGTTAVDLAVDKFYERVLQ-DDRIKHFFA-------------DVDMAKQRAHQKAFL
TETRAHYMENA: ----------------MNKPQTIYEKLGGENAMAKAAPLFYKKVLA-DERVKHFFK-------------NTDMDHQTKQQTDFL
CHLAMYDOMON: PSTSATAAAATAPAPARKCPSSLFAKLGGREAVEAAVDKFYNKIVA-DPTVSTYFS-------------NTDMKVQRSKQFAFL
PARAMECIUM : ---------------------MSLFEQLGGQAAVQAVTAQFYANIQA-DATVATFFN-------------GIDMPNQTNKTAAFL
NOSTOCCOMMU: -------------------MSTLYDNIGGQPAIEQVVDELHKRIAT-DSLLAPVFA-------------GTDMVKQRNHLVAFL
MYCOBACTERI: --------MGLLSRLRKREPISIYDKIGGHEAIEVVVEDFYVRVLA-DDQLSAFFS-------------GTNMSRLKGKQVEFF

                EEEEE        FFFFFFFFF         GGGGGGGGGGGGGGGGGGG     HHHHHHHHHHHHHHHHHHHHHHHHHH
                11112        123456789         12345678911111111111     12345678911111111112222222
                67890                                    0123456789              01234567890123456
MYOGLOBIN  : GAILKKKGHHEAELKPLAQSHATKH---KIPIKYLEFISEAIIHVLHSRHPGDFGADAQGAMNKALELFRKDIAAKYKELGYQG
                       6         7         8         9         10        11        12
                       0         0         0         0         0         0         0
SYNECHOCYST: TYAFGGTDK--YDGHYMREAHKELVENHGLNGEHFDAVAEDLLATLKEM--GVPEDLIAEVAAVAGAPAHKRDVLNQ-------
TETRAHYMENA: TMLLGGPNH--YKGKNMTEAHKGMN----LQNLHFDAIIENLAATLKEL--GVIDAVINEAAKVIEHTRKDMLGK---------
CHLAMYDOMON: AYALGGASE--WKGKDMRTAHKDLV--PHLSDVHFQAVARHLSDTLTEL--GVPPEDITDAMAVVASTRTEVLNMPQQ------
PARAMECIUM : CAALGGPNA--WTGRNLKEVHANMG----VSNAQFTTVIGHLRSALTGA--GVAAALVEQTVAVAETVRGDVVTV---------
NOSTOCCOMMU: AQIFEGPKQ--YGGRPMDKTHAGLN----LQQPHFDAIAKHLGERMAVR--GVSAENTKAALDRVTNMKGAILNK---------
MYCOBACTERI: AAALGGPEP--YTGAPMKQVHQGRG----ITMHHFSLVAGHLADALTAA--GVPSETITEILGVIAPLAVDVTSGESTTAPV--
```

FIGURE 1: Primary structure of the globin from *Synechocystis* sp. PCC 6803 (SYNECHOCYST; gene slr2097, *glbN*) compared to other truncated hemoglobins: TETRAHYMENA, myoglobin (hemoglobin) from *Tetrahymena pyriformis*; CHLAMYDOMON, globin LI637 (gene *LI637*) from *C. eugametos*; PARAMECIUM, myoglobin (hemoglobin) from *P. caudatum*; NOSTOCCOMMU, cyanoglobin from *N. commune* UTEX 584 (gene *glbN*); MYCOBACTERI, hypothetical 14.5 kDa protein cy48.23 (gene mtcy48.23, *glbN*) from *Mycobacterium tuberculosis*. The first sequence (MYOGLOBIN) is that of sperm whale (*Physeter catodon*) myoglobin. The top lines indicate helix denominations in this protein. The numbers above the *Synechocystis* sp. PCC 6803 sequence indicate every 10 residues in that structure. The initial Met is cleaved from the expressed protein. The proximal histidine (F8) is in bold face in all sequences.

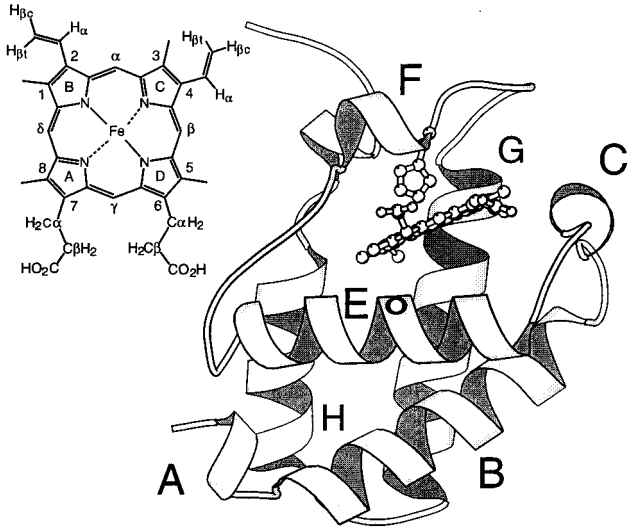

FIGURE 2: (A, right) The truncated hemoglobin fold observed in *C.eugametos* hemoglobin in the metcyano form (1dly.pdb; *11*). The circle on the E helix indicates the position of residue E10. In this protein, the side chain points upward and away from the iron ion. (B, left) The heme structure with Fischer nomenclature is shown to the left of the ribbon.

Presumably, some of these help to maintain the heme in its site and reshape the cavity to protect the prosthetic group from excessive water access. In contrast to the full-length globins, trHb's share a tendency to coordinate the iron atom with two, rather than one, protein ligands (*12*−*14*). One of these is the "proximal" histidine as in other globins; the second has been identified in *C. eugametos* as Tyr B10 (*6*). However, variants of trHb's are capable of recruiting alternative residues for coordination (*14*), and this behavior suggests that conformational rearrangement of the heme site is facile in these proteins.

Here, the characterization of trHb from the cyanobacterium *Synechocystis* sp. PCC 6803 (S6803 rHb, where "r" indicates the recombinant origin of the protein) was pursued. In previous work (*15*), it was shown that the apoprotein binds ferric heme [Fe(III) protoporphyrin IX] and produces a low-spin hexacoordinated species, or hemichrome, with optical and NMR spectra resembling those of cytochrome b_5, a protein in which the heme is coordinated by two histidines. Reduction of ferric S6803 rHb with dithionite yields an Fe(II) complex exhibiting spectral features consistent with hexacoordination as well. The goals of the present study were to identify the sixth ligand to the iron ion, as this information is critical to understanding the chemical and functional properties of the protein and to guide future in vivo investigations. In addition, some of the consequences of hexacoordination were investigated to begin the comparison to other globins and cytochromes, both natural and artificial.

MATERIALS AND METHODS

Materials. All chemicals were purchased from Sigma (St. Louis, MO) and enzymes from Promega Corp. (Madison, WI), except where otherwise indicated.

S6803 rHb. The apoprotein was prepared by a modification of the published protocol (*15*) to utilize the protein packed in inclusion bodies (see Supporting Information). The yield was 35−40 mg of pure apoprotein/L of growth medium. This protein had the same properties as that obtained from the soluble fraction. Uniformly labeled apoprotein (^{15}N and ^{15}N−^{13}C) was similarly purified from cells grown in modified M-9 medium containing $^{15}NH_4Cl$ and [^{13}C]glucose (Isotec, Miamisburg, OH) as appropriate. The ferric form of S6803 rHb was prepared by reconstitution as previously reported (*15*). If necessary, the holoprotein was dialyzed against dd H_2O to remove buffer, and the protein was lyophilized for long-

term storage. Lyophilization did not alter the spectroscopic or thermodynamic properties of the protein.

Apoprotein Extinction Coefficient. The extinction coefficient of apoHb was determined at pH 8.0 by the method of Gill and von Hippel (*16*). The extinction coefficient at 278 nm was calculated to be 7.36 mM^{-1} cm^{-1} for the folded apoprotein on the basis of a compositional value of 7.00 mM^{-1} cm^{-1} for the unfolded protein.

Heme:Protein Stoichiometry. The number of heme molecules incorporated in each molecule of S6803 apoHb was obtained by the method of Antonini and Brunori (*17*). A break in the titration curve occurred within experimental error of equivalence and confirmed the 1:1 stoichiometry of the reconstituted material (Figure S1, Supporting Information).

Holoprotein Sample Purity. Freshly reconstituted ferric S6803 rHb had a mass consistent with expectations (*15*) and yielded reproducible NMR spectra. After days to weeks in solution, some of the samples underwent an apparently irreversible modification altering the chemical shift of heme and protein resonances. This transformation was accompanied by minor changes in the optical spectrum. The transformed protein was subjected to the hemochromogen assay (*18*) with results identical to those obtained with the freshly prepared holoprotein. However, the heme remained tightly associated with the protein matrix both at low pH and through the procedure for MALDI analysis. In view of this occasional conversion to a different low-spin species, all holoprotein samples were subjected to an NMR control before use.

Isoelectric Point Determination. The p*I* of apo and holo S6803 rHb was experimentally determined by use of the Pharmacia Phast System with precast Phast IEF 4-6.5 gels, according to the manufacturer's instructions (Amersham Pharmacia Biotech, Inc., Piscataway, NJ) and with comparison to IEF protein standards (Sigma). The measured apoprotein p*I* was 4.9, close to the theoretical value of 5.2 calculated from the primary structure with Proteomics tools of ExPASy molecular biology server. The p*I* of the ferric holoprotein was 4.4. The soluble domain of rat hepatic cytochrome b_5 in the oxidized state and in the apoprotein state (prepared as described in ref *19*) exhibited a similar difference. All S6803 Hb NMR data were collected at pH values above the p*I*.

Circular Dichroism. Apoprotein CD spectra were collected at 25 °C from 190 to 300 nm on an Aviv Model 62 DS circular dichroism spectropolarimeter. The concentration of the samples was 20 μM protein in 20 mM phosphate buffer (pH 7.2). Raw data were collected with 5 s averaging and corrected for buffer contribution. The molar residual ellipticity (MRE in mdeg cm^2/dmol) was calculated as previously reported (*15*). The holoprotein CD spectrum was collected in the Soret region from 360 to 460 nm on two samples (65 and 75 μM) with remaining parameters as above.

Holoprotein Thermal Denaturation. Absorbance spectra were collected on an Aviv Model 14D spectrophotometer with Pelletier device for rapid temperature adjustment. Typically, a holoprotein solution of 5.8 μM in 20 mM phosphate buffer (pH 7.2) was heated from 5 to 89 °C in 2 °C steps, and spectra were collected between 260 and 440 nm after an equilibration period of 3 min. Reversibility was inspected by refolding the protein from 75 to 5 °C, collecting spectra at 5 °C intervals. The absorbance at 410 nm was plotted as a function of temperature and fitted using NFIT (University of Texas, Galveston, TX) to obtain the apparent midpoint of the transition (T_m) according to the van't Hoff equation adapted for the dependence of the fully folded and fully unfolded signals on temperature (*20*).

NMR Spectroscopy. Samples of oxidized reconstituted recombinant S6803 rHb ranged in concentration from 0.6 to 2 mM in buffer as specified. The pH was adjusted using HCl or NaOH. The ^{1}H spectra were referenced to the water resonance at 4.76 ppm; ^{13}C signals and ^{15}N signals were referenced indirectly to the proton frequency (*21*).

NMR data were acquired on a Bruker DRX-600 spectrometer (14.1 T, operating at a ^{1}H frequency of 600.13 MHz). Homonuclear experiments (2QF-COSY, TOCSY, and NOESY) were carried out as reported elsewhere (*15*). Triple resonance 3D experiments were performed on a ^{13}C−^{15}N-labeled sample (20 mM phosphate, pH 7.5) with the following parameters for dimensions t_1, t_2, and t_3, respectively, with the asterisk indicating the number of complex data points: HCCH-TOCSY and COSY (^{1}H, 4808 Hz, 64*; ^{13}C, 11468 Hz, 40*; ^{1}H, 4808 Hz, 512*) (*22*); ^{1}H−^{13}C HSQC-NOESY (^{1}H, 8013 Hz, 64*; ^{13}C, 11468 Hz, 32*; ^{1}H, 8013 Hz, 512*) (*23*); HNCA (^{15}N, 2222 Hz, 44*; ^{13}C, 5000 Hz, 48*; ^{1}H, 8013 Hz, 512*) (*24*, *25*), and CBCA(CO)NH (^{13}C, 8929 Hz, 60*, ^{15}N, 2222, 24*; ^{1}H, 8013, 512*) (*26*). In addition, ^{1}H−^{15}N TOCSY-HSQC and ^{1}H−^{15}N NOESY-HSQC data (modified from ref *27*) were collected on a uniformly ^{15}N-labeled sample. Parameters were as follows: ^{15}N, 2554 Hz, 128*; ^{1}H, 13020 Hz, 2048*. In all of these experiments, quadrature detection in the indirect dimensions was achieved using the TPPI−States method (*28*), and a WATERGATE solvent suppression scheme was used (*29*, *30*).

Data sets were processed using FELIX 97.0 (Molecular Simulations Inc., San Diego, CA). In general, the FID along the direct dimension was convoluted with a low-order polynomial to remove the residual water signal before filtering with a sine-squared window function phase-shifted by 40−60°. Along the indirect dimensions, the interferograms were extended by linear prediction before apodizing with a sine-squared window function phase-shifted by 60−90°. Final data set sizes were typically 512−1024 × 64−128 × 128 real data points.

^{1}H WEFT spectra (*31*) were collected in ^2H_2O over a spectral width of 24510 Hz and 4096 data points (acquisition time of 84 ms) (*32*). After a 3 ms relaxation delay, a composite 180° pulse was applied for nonselective inversion. This pulse was followed by an adjustable recovery period. ^{1}H WEFT NOE data were obtained in 95% ^1H_2O/5% ^2H_2O over the same spectral width and number of data points as above. In this case, the relaxation delay was 100 ms. A single 180° pulse was applied and followed by a recovery period of 300 ms. During the last 30 ms of this period, a low-power rf pulse was applied either to the resonance of interest or to a reference position. The water signal was suppressed with low-power presaturation during the relaxation delay and the WEFT delay. To obtain the data shown in Figure 7, a total of 18432 transients were collected in blocks of 1024. For processing, the water line was minimized with a convolution difference filter; an exponential line broadening of 50 Hz was applied prior to transformation. ^{1}H WEFT NOESY data were collected on this sample with 1024 complex points in the direct dimension and 512 real points in the indirect

dimension and TPPI quadrature detection. The relaxation time was 50 ms, the WEFT delay 250 ms, and the mixing time 30 ms. A total of 256 transients were accumulated for each time increment. Data processing included a convolution difference removal of the water line, square cosine bell multiplication, and zero filling to a 2048 × 2048 real matrix.

The nonselective T_1 of C-bound protons was measured by standard inversion recovery methods. The nonselective T_1 of N-bound protons was determined using a fast HSQC sequence (*33*). Inversion of the ^{1}H amide region was achieved with a 3-9-19 pulse train. T_1 values were obtained by measuring cross-peak height as a function of recovery time and fitting with a single exponential decay. An estimate of the efficiency of the inversion was obtained by comparing the extrapolated zero time intensity to the fully relaxed intensity. WATERGATE ^{1}H−^{15}N HSQC experiments with and without saturation at the water frequency were carried out to determine the saturation factor of the resonances whose T_1 was of interest to this work. Saturation of the water line and underlying resonances led to a reduction of intensity of less than 10% for His46 and His70 peptide NH's and ring NδH's.

Nonselective T_1 values were translated into proton-to-iron distances (R_{i-Fe}) by scaling with the T_1 value of a hypothetical heme methyl group ($R_{Me-Fe} \sim 6.2$ Å) experiencing no contribution from delocalized spin density (*34*). To estimate this T_1 value, $1/T_1$ for the 5-, 1-, and 8-CH_3 (Table 3 and ref *15*) were plotted versus $(\delta_{obs} - \delta_{dia} - \delta_{dip})^2$, where δ_{obs} is the chemical shift of the methyl group, δ_{dia} is the diamagnetic shift (assumed to be +3.5 ppm; *35*), and δ_{dip} represents the axial dipolar shift due to the magnetic anisotropy $\Delta\chi_{ax}$ (*34*). In the absence of a $\Delta\chi_{ax}$ estimate, δ_{dip} was set to zero and a reference $T_{1,Me}$ of 270 ms was obtained and used; inclusion of a δ_{dip} term of −3 ppm (a representative contribution for sperm whale metMbCN; *35*) raised this value to 300 ms. Approximate distances in angstroms were calculated with $(T_{1,i}/T_{1,Me})^{1/6} = R_{i-Fe}/6.2$. For axial residues, these distances are likely to be slightly underestimated (*36*).

Kinetics of Heme Reorientation by NMR Spectroscopy. NMR samples were prepared by dissolving lyophilized apoprotein in 20 mM phosphate buffer (H_2O, pH 7.2) to a concentration of 1 mM. Hemin was dissolved in cold 0.1 M NaOH and stirred at 4 °C in the dark for at least 30 min. The appropriate amount of hematin solution (1 equiv/10 μL) was added to the apoprotein solution contained in the NMR tube and mixed rapidly before insertion in the magnet, with the probe and bore tube preequilibrated at the desired temperature, calibrated with ethylene glycol or methanol (*27*). The experiments were performed at 5, 15, 25, 30, and 35 °C. The reaction at 5 °C was too slow for determination of an accurate rate constant. To confirm heme disorder, a sample was reconstituted with 2,4-dimethyldeuteroporphyrin IX (Porphyrin Products, Logan, UT) and monitored at 25 °C.

^{1}H NMR spectra were recorded over a spectral width of 24 kHz. The water signal was suppressed with low-power irradiation for 1.2 s. The number of transients and the time delay between each time point were adjusted in order to obtain reliable target peak intensities. Data were processed with 25 Hz exponential broadening using the Bruker software XWINNMR.

Heme reorientation can be represented as

$$\mathrm{m} \underset{k_b}{\overset{k_f}{\rightleftharpoons}} \mathrm{M} \quad (1a)$$

(*37*) where m is the minor isomer (least populated at equilibrium), M is the major isomer (most populated at equilibrium), and k_f and k_b are forward and backward unimolecular rate constants, respectively. Heme transfer experiments (see below) indicate that minor and major isomers undergo heme loss that can contribute to the equilibration

$$\mathrm{m} \underset{k_2^{m}}{\overset{k_1^{m}}{\rightleftharpoons}} \mathrm{apoHb} + \mathrm{heme} \quad (1b)$$

$$\mathrm{M} \underset{k_2^{M}}{\overset{k_1^{M}}{\rightleftharpoons}} \mathrm{apoHb} + \mathrm{heme} \quad (1c)$$

The initial rate of heme insertion into the apoprotein was modeled with two irreversible reactions

$$\mathrm{apoHb} + \mathrm{heme}' \xrightarrow{k_i^{M}} \mathrm{M} \quad (1d)$$

$$\mathrm{apoHb} + \mathrm{heme}' \xrightarrow{k_i^{m}} \mathrm{m} \quad (1e)$$

accounting for the slow formation of M and m upon mixing. This scheme distinguished competent ferric heme as in eqs 1b and 1c from a slowly inserting ferric heme species (heme′).

The rate of equilibration was determined by integrating resolved peaks representative of each isomer. The peak area was then assigned a time value coinciding with the center of the time interval during which the transients for that data point were acquired. The programs KinSim and KinFit (*38*, *39*) were used to fit simultaneously the decay of m and the buildup of M. At 25 °C, the bimolecular rate constants k_2^m and k_2^M were fixed to 1×10^8 M^{-1} s^{-1} (*40*), and k_1^M and k_1^m were set to a value consistent with the rate constant of heme loss determined optically (see below, $k_1^M = k_d$ in eq 2a) and according to microscopic reversibility (see Discussion, $k_1^m \sim (k_f/k_b)k_1^M$). The rate constants k_i^m, k_i^M, k_f, and k_b were optimized by the fit. The activation energy of the intramolecular reaction in the forward direction was determined by applying the Arrhenius equation $\ln k_f = \ln A - E_a/RT$, where A is the preexponential factor, E_a, the activation energy, R, the gas constant, and T, the temperature in kelvin.

Heme Release from Oxidized S6803 rHb. The kinetics of heme release to equine apomyoglobin were followed by NMR and optical spectroscopy at 25 °C. The optical procedure was as reported previously (*15*) with a S6803 rHb concentration of 65 μM (all holoprotein concentrations are reported on a per heme basis) and a 3-fold excess of apomyoglobin in 20 mM potassium phosphate at pH 7.2. The absorbance at 634 nm, containing a negligible contribution from S6803 rHb, was measured as a function of time. To obtain estimates for the rate of loss, the data were simulated and fitted with the programs KinSim and KinFit (*38*, *39*) using a mechanism including the following steps:

$$\mathrm{Hb} \underset{k_r}{\overset{k_d}{\rightleftharpoons}} \mathrm{apoHb} + \mathrm{heme} \quad (2a)$$

$$\mathrm{Hb}' \xrightarrow{k_d'} \mathrm{apoHb} + \mathrm{heme} \quad (2b)$$

$$\mathrm{apoMb} + \mathrm{heme} \underset{k_d''}{\overset{k_r}{\rightleftharpoons}} \mathrm{Mb} \quad (2c)$$

In these equations, Hb represents the fraction of S6803 rHb that loses the heme slowly, and Hb′, that which loses it rapidly and irreversibly. The optical method does not resolve the M and m isomers, and the nature of Hb and Hb′ cannot be determined from these data. The apparent bimolecular rate constant for heme insertion into an apoprotein, k_r, was set to 1×10^8 M^{-1} s^{-1} (*40*) and the rate constant for heme loss by Mb, k_d'', to 1.7×10^{-5} s^{-1} (*41*). The relative signal amplitude from S6803 rHb and S6803 rHb′ and the first-order rate constants k_d and k_d' were optimized. The results were insensitive to variations of k_d'' within a range consistent with experimental error (*42*). The model given by eqs 2 does not require contact between the donor and acceptor proteins (*43*) and assumes that Hb and Hb′ do not interconvert on the time scale of the heme release. Further complexity was added to the mechanism by taking into account heme orientational disorder (eqs 1b and 1c and text). Moderate changes to the fitted constants followed. The numbers in the text are estimates based on the simulations.

The NMR procedure used an ~1 mM solution of oxidized holo S6803 rHb to which was added a 3-fold molar excess of freshly prepared equine apomyoglobin (*44*). Final conditions were 10 mM Tris and pH 6.9. The heme transfer reaction was monitored by collecting 1D NMR spectra at regular time intervals. The spectral width was set to 100 000 Hz in order to observe S6803 rHb and the metaquoMb signals. Data were processed with 25 Hz exponential line broadening. The intensity of resolved heme signals from S6803 rHb was followed as a function of time, and the profiles were analyzed as above.

Electrochemistry. Holoprotein was diluted to a concentration of approximately 100 μM in thoroughly degassed 50 mM Tris, pH 8.0, or 100 mM sodium phosphate, pH 7.1, at room temperature. Poly-L-lysine was tested for its ability to promote electron transfer at the electrode surface at concentrations ranging from 0.1 to 0.8 mM in 0.1 or 0.2 mM increments in the phosphate buffer. The reduction potential was measured directly by Osteryoung square-wave voltammetry (OSWV; *45*) on a BAS 100B electrochemical analyzer (Bioanalytical Systems, West Lafayette, IN) utilizing a BAS cell stand C3 equipped with a glassy carbon working electrode, a platinum auxiliary electrode, and a silver/silver chloride reference electrode filled with 3 M NaCl (Bioanalytical Systems). The working electrode required polishing with wet alumina, flanked by consecutive dd H_2O and methanol rinses, immediately before each measurement. Following a 2 s equilibration delay at initial conditions, reduction potentials were collected over a range of +400 mV up to −1100 mV (versus Ag/AgCl reference) at a sensitivity of 10 μA/V, with a step size of 4 mV, and a square-wave amplitude of 25 mV and frequency of 15 Hz. Solutions were blanketed with nitrogen gas at all times and stirred during potential measurement. Peak potentials were detected by BAS 100W software version 2.3, and resulting values were corrected to yield reduction potentials versus the standard hydrogen electrode (SHE) by adding 206 mV as supplied by the manufacturer.

RESULTS

Identification of the Axial Ligands to the Iron Atom. According to sequence alignments (Figure 1) and the structure of the related *C. eugametos* and *P. caudatum* hemoglobins (*11*), His70 serves as the proximal histidine in S6803 rHb. The distal ligand in the hemichrome could be one of several possibilities among lysine, methionine, tyrosine, or histidine, as each of these is found at potentially suitable positions. Recent mutagenesis studies (*46*) implicate the histidine at position E10. To identify the protein ligands in the wild-type protein, apo S6803 rHb was uniformly labeled with ^{15}N and ^{13}C for triple resonance NMR experiments. With a combination of heteronuclear and homonuclear data, nearly complete assignments were achieved (C. J. Falzone et al., unpublished results). Relevant to this study is the portion of HNCA data extending from Ala41 to Leu51 (in the E helix, Figure 1). This portion is shown in Figure 3 to illustrate the quality of the spectra in the proximity of the low-spin heme iron. In this data set, the Cα signal of His46 was folded from its downfield-shifted position of 80.1 ppm to an apparent chemical shift of 47 ppm. Complete sequential analysis revealed that His70 had a Cα signal shifted to 70.7 ppm. CBCA(CO)NH data yielded Cβ shifts of 25.1 ppm (His46) and 25.4 ppm (His70). HCCH and homonuclear TOCSY and COSY data assigned the attached protons. Figure 4 presents the 25.1 ppm carbon plane of the $^1H-^{13}C$ HSQC NOESY data, which contains these signals and some of their NOEs.

Within a few angstroms of the iron ion, the nonselective proton T_1 parameters are dominated by dipolar paramagnetic

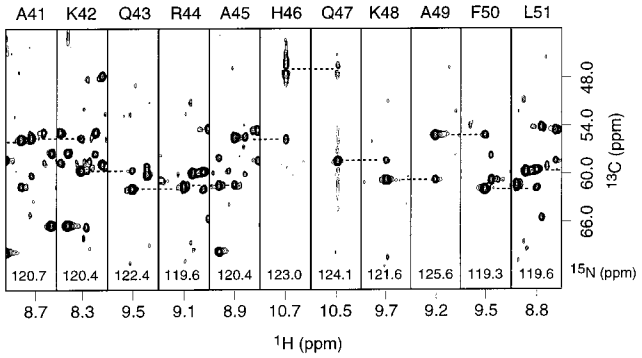

FIGURE 3: Sections of an HNCA experiment collected on uniformly $^{15}N-^{13}C$-labeled ferric S6803 rHb in 95% ^1H_2O/5% ^2H_2O, pH 7.5, and 20 mM phosphate. The probe temperature was 25 °C. The sequential connectivities are shown from residue Ala41 to residue Leu51. The ^{15}N frequency of each panel is indicated at the bottom. Alanines at positions 41, 45, and 49 facilitated unambiguous assignment through their characteristic Cβ shift. The Cα resonance of His46 occurs at ~80.1 ppm and is folded in at ~47 ppm.

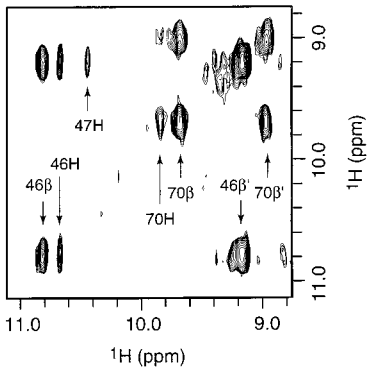

FIGURE 4: Plane of the ^{13}C-separated NOESY collected on the same sample. The data are located at a ^{13}C frequency of 25.1 ppm and contain the connectivities for the Cβ of both His46 and His70.

Table 1: Chemical Shift and T_1 Values for His46 and His70 in Ferric S6803 rHb

residue	nucleus	δ (ppm)[a]	T_1 (ms)[b]
His46	N*H*	10.67	260
	Cα*H*	7.70	
	Cβ*H*	10.82	90
	Cβ*H*′	9.20	110
	Nδ*H*	13.2	45
	Cϵ*H*	−11.6	3.7
	N	123.0	
	Nδ	131.0	
	Cα	80.1	
	Cβ	25.9	
His70	N*H*	9.90	170
	Cα*H*	6.75	
	Cβ*H*	9.72	140
	Cβ*H*′	8.92	230
	Nδ*H*	15.0	38
	N	113.0	
	Nδ	136.0	
	Cα	70.7	
	Cβ	25.4	

[a] Measured in 95% H_2O/ 5% ^2H_2O, pH 6.9−7.5, at 25 °C. [b] Measured either in 95% H_2O/5% ^2H_2O, pH 7.2, at 25 °C with a modified HSQC experiment or in 99% ^2H_2O by inversion recovery. In all cases, only points within the first 100 ms of recovery were used.

contributions and depend on R^6, where R is the H−Fe distance (*32*, *34*). An estimate of R can be obtained by comparing T_1 values to a suitable reference. The T_1 parameters of the shifted β protons of His46 and His70, when compared to that of a heme methyl group, indicated distances to the paramagnetic center between 5 and 6 Å. Chemical shifts and T_1 values are listed in Table 1.

In addition to the backbone NH and side-chain NH_2 cross-peaks, the $^1H-^{15}N$ HSQC spectrum of ferric S6803 rHb (Figure S2, Supplementary Information) contained two side-chain outliers at $^1H-^{15}N$ chemical shifts of 15 ppm (labeled with c in ref *15*) and 136 ppm and of 13.2 ppm (labeled with e) and 131 ppm. The T_1 values for these were ∼40 ms (Table 1) and suggested a distance of ∼4.5 Å to the iron. WEFT-NOESY data (Figure 5) revealed that the proton responsible for signal c was in dipolar contact with one of the Cβ*H*′s of His70 whereas the proton giving rise to signal e was close to one of the Cβ*H*′s of His46. As the paramagnetic relaxation is expected to limit detectable NOEs to short-range intraresidue effects, c was assigned to the Nδ*H* of His70 and e to the Nδ*H* of His46.

Axial coordination of an imidazole ring through the Nϵ atom brings Cδ*H* and Cϵ*H* within 3.2−3.5 Å of the iron. As a result, in paramagnetic species both Cδ*H* and Cϵ*H* exhibit short T_1's and broad resonances. In favorable cases, these resonances are detected by suppressing the signals of other protons with accelerated recycling time following an inversion recovery scheme (*32*; WEFT spectrum) as shown in Figure 6. In this ^2H_2O spectrum, several nonexchangeable signals are emphasized, among which m, n, o, and z have a line width in excess of 300 Hz. Proton z was found to have a T_1 of ∼4 ms at 25 °C (*15*), and although the T_1 of protons m, n, and o could not be determined directly, variable delay WEFT experiments indicated values similar to that of z. To identify z, 1D NOE difference data were collected with a WEFT sequence. A single effect was obtained to peak e (Figure 7), which implied that z is the ring Cϵ*H* of His46. Thus, of m, n, and o, one signal is likely to arise from the

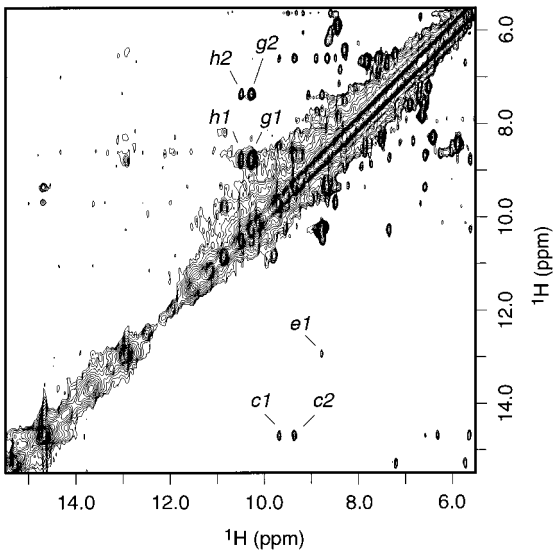

FIGURE 5: Portion of a ^1H WEFT-NOESY experiment collected on ferric S6803 rHb in 95% ^1H_2O/5% ^2H_2O, pH 7.8, and 10 mM Tris. The probe temperature was 35 °C. The mixing time was 30 ms (see Materials and Methods for experimental details). The figure emphasizes the NOEs of the exchangeable nitrogen-bound protons at 15 ppm (c) and 13 ppm (e). Resonance c displays NOEs to 9.67 ppm (c1) and 9.35 ppm (c2). These signals are assigned to the NH and the low-field CβH of His-70, respectively. Resonance e displays NOE to 8.8 ppm (e1) assigned to the high-field CβH of His46. The sets of NOE and the T_1 values (see text) support assignment of c to the ring NδH of His70 and e to the ring NδH of His46. Also marked are cross-peaks from His46: h1, His46 NH to CβH′; g1, His46 CβH to CβH′; h2, His46 NH to His46 CαH; g2, His-46 CβH to His46 CαH.

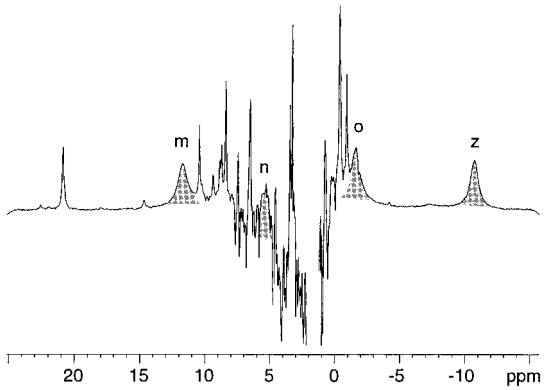

FIGURE 6: Representative ^1H WEFT NMR spectrum of ferric S6803 rHb at 600 MHz. The protein (600 μM heme) was in ^2H_2O, buffered at pH 7.2 with 20 mM Tris. The probe temperature was 35 °C. The recovery delay following inversion was 60 ms, and the recycling rate was ∼7 s^{-1}. The time-domain data were subjected to a line broadening of 20 Hz prior to transformation. With this set of parameters, several signals have experienced partial recovery and give rise to positive intensity. The shaded peaks m (11.7 ppm), n (5.4 ppm), o (−1.7 ppm), and z (−10.8 ppm) have relaxed completely; their line width and short T_1 identify them as belonging to the axial residues.

Cδ*H* of His46 and the other two from the Cδ*H* and Cϵ*H* of His70.

In support of the bishistidyl ligation of the heme in the ferric state of S6803 rHb, the chemical shifts and H−Fe distances of the axial histidines in the ferric form of cytochrome b_5 (*47*, *48*) and cytochrome *c* (*49*) are consistent with the values for His70 and His46 listed in Table 1. Furthermore, no other candidate, for example, Tyr22 (B10)

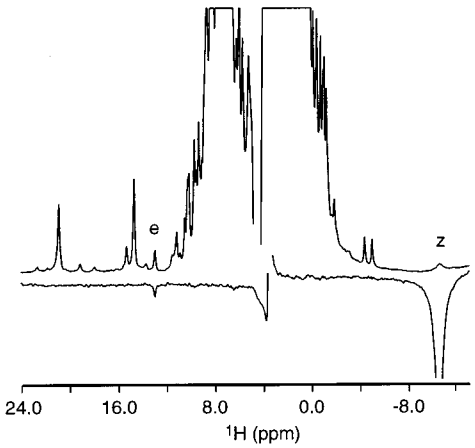

FIGURE 7: ^{1}H NOE data collected on the same sample as used for Figure 5. The top spectrum was acquired with water saturation and a recycling rate of ~0.6 s^{-1}. The bottom trace represents a difference spectrum obtained in a WEFT-NOE experiment where the shifted peak z at −10.6 ppm was irradiated. The strong signal at 3.6 ppm arises from the Tris buffer. A single NOE is obtained to peak e at 13 ppm. This identifies z as the CϵH of His46.

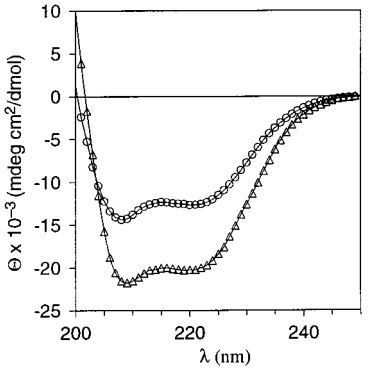

FIGURE 8: Changes in the far-UV circular dichroism spectrum of S6803 rHb induced by heme binding at pH 7.2 (20 mM phosphate) and 25 °C. Apoprotein (○) and holoprotein (△) samples were ~20 μM protein or heme. The increase in molar residual ellipticity indicates that heme binding contributes an additional ~30% to the helical content of the protein.

and Met40 (E4), displayed shifts and relaxation parameters indicative of ligation to the iron. To begin the analysis of the consequences of bishistidyl coordination and the comparison of S6803 rHb to its truncated and full-length relatives, several aspects of the interactions between heme and protein matrix were characterized at neutral pH.

Conformational Changes Following Heme Insertion. The ^{1}H NMR spectrum of apo S6803 rHb at 1 mM concentration and neutral pH was broad and exhibited little chemical shift dispersion (data not shown). Under these experimental conditions, the polypeptide chain did not appear to adopt extensive tertiary structure. However, the far-UV CD spectrum shown in Figure 8 indicated the presence of helices. Addition of hemin in a 1:1 ratio caused a near doubling of helical content, also shown in Figure 8.

The reconstitution reaction was monitored by ^{1}H NMR spectroscopy to confirm the identity of the product observed by optical methods. In this experiment, 1 equiv of hemin is mixed into the apoHb solution, and the proton spectrum is collected at regular time intervals following the addition. The first spectrum obtained after adjustment of the pH is shown in Figure 9. It contained two sets of resonances and it

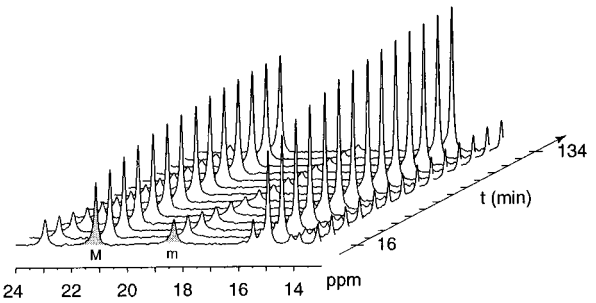

FIGURE 9: Downfield region of the 600 MHz ^{1}H NMR spectrum of freshly reconstituted oxidized S6803 rHb (pH 7.2, 20 mM phosphate buffer, 30 °C). Peaks M and m arise from two different heme orientational isomers, related by a 180° rotation about the $\alpha-\gamma$ meso axis.

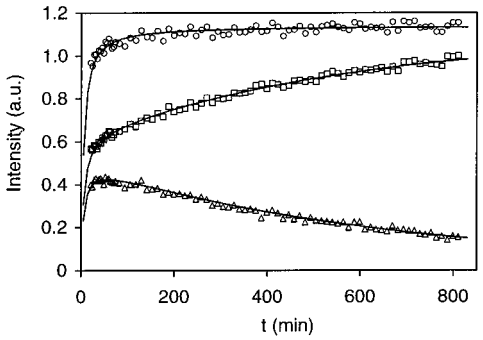

FIGURE 10: Time course of the integrated area of Figure 9 peaks M (□), m (△), and their sum (○) at 15 °C. The lines through the data points are the results of fits to the mechanism described by eq 1a−e.

changed with time, the first set of resonances (represented by heme methyl peak M) gaining intensity at the expense of the second set (represented by heme methyl peak m). Set M corresponds to the hemichrome spectrum reported previously (*15*). Spectral changes such as those depicted in Figure 9 are typical of heme reorientation following heme addition to apo *b* heme proteins. The reorientation is, to a good approximation, a reversible rotation of the prosthetic group by 180° about its $\alpha-\gamma$ meso axis (*50*). Accordingly, reconstitution with 2,4-dimethyldeuteroporphyrin IX, which is symmetrical with respect to the $\alpha-\gamma$ meso axis, yielded time-independent spectra (not shown).

The integrated areas of M and m were fitted to a kinetic model including irreversible and reversible heme insertion steps to produce each of the two isomers as well as their equilibration through an intramolecular step (eqs 1). Sample data are shown at 15 °C in Figure 10. At this temperature, the slow production of the holoprotein manifested in a rise of the sum of peaks M and m during the early stages of equilibration. This was attributed in part to the disaggregation of hematin (*51*), but a simple heme dimer disruption step did not yield a satisfactory fit of the data, and reactions described by eqs 1d and 1e were used instead.

The forward rate constants for equilibration (k_f in eq 1a) are listed in Table 2 and plotted as a function of inverse temperature in Figure 11. An activation energy of 132 ± 4 kJ/mol and a preexponential factor of 2×10^{19} s^{-1} were obtained from this plot. At equilibrium, the minor form concentration was only a few percent and increased slightly with temperature. It was not possible to obtain a reliable numerical value for $\Delta H°$ because of the large error in the reverse reaction rate constants and equilibrium constants.

Table 2: Parameters for Heme Reorientation in Ferric S6803 rHb at pH 7.2

temp (K)	k_f ($\times 10^4$ s^{-1})[a]
288.2	0.26
298.2	1.4
303.2	3.4
308.2	9.8

[a] Error of the fit is at most 4%.

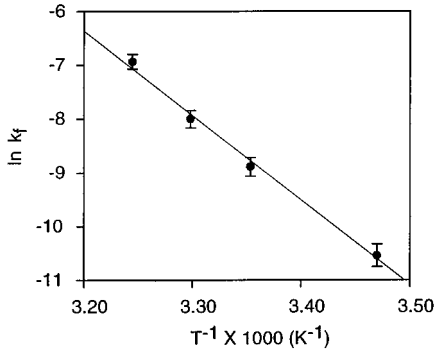

FIGURE 11: Arrhenius plot for heme reorientation within S6803 rHb (pH 7.2). The individual rate constants (k_f) were obtained from data for peak M as shown in Figure 10.

Kinetics of Heme Transfer. S6803 rHb has among its closest relatives the cyanoglobin from *Nostoc commune* (GlbN). This protein loses its heme group readily, but it is not known whether the lower affinity is a property shared by trHb's in all of their complexation states. The kinetics of heme loss from the oxidized state of S6803 rHb at 25 °C were studied optically and by NMR spectroscopy. The second method has the advantage of identifying the products whereas the first can be performed at lower concentrations. Heme release was found to be biphasic (Figure S4, Supporting Information). The major fraction (>90%) of the S6803 rHb signal disappeared with a rate constant of ~0.01 h^{-1}, whereas the remainder of the signal decayed with a rate constant of ~0.5 h^{-1}. NMR spectroscopy, which monitored the intensity of the S6803 rHb heme signals, also showed a biphasic decrease, with the slow phase contributing <10% of the total intensity.

Heme Orientation in S6803 rHb. The heme group in the low-spin state gives rise to several resolved ^1H resonances (*15*). These were assigned to specific substituents of the porphyrin ring by relying on the sole intermethyl NOE, between the 1-CH_3 and the 8-CH_3 (Figure 2 inset). In the WEFT-NOESY data, such an NOE was detected at 15.1 and 10.4 ppm. The 15.1 ppm signal was identified as the 1-CH_3 through its NOEs to a vinyl side chain. Other assignments were derived from this one to provide the list in Table 3.

With known heme and backbone signals, the ring resonances of the strictly conserved phenylalanine at position CD1 (Phe35) could be assigned at 7.66 ppm (δ), 8.59 ppm (ϵ), and 6.61 ppm (ζ) using NOE and 2QF-COSY data. The peak at 6.61 ppm was broad and unresolved from the diamagnetic envelope. In all globins of known structure, Phe CD1 is located on one side of the porphyrin ring, in contact either with pyrroles A and B or with pyrroles C and D. In S6803 rHb, Phe35 has weak NOEs to the 5-CH_3 (pyrrole D), establishing that at equilibrium the heme orientation in its binding site is identical to that in mammalian myoglobins

Table 3: ^1H NMR Parameters for Heme Resonances in the Spectrum of Ferric S6803 rHb

δ (ppm)[a]	assignment	signal[b]
21.27	5-methyl	a
15.54	2-α-vinyl	b
15.07	1-methyl	d
10.37	8-methyl	j
9.98	3-methyl	l
6.84	4-α-vinyl	
−1.67	*trans*-4-*β*-vinyl	v
−2.14	*cis*-4-*β*-vinyl	w
−4.54	*trans*-2-*β*-vinyl	x
−5.15	*cis*-2-*β*-vinyl	y

[a] Refer to Figure 2B for the heme structure. In 95% ^1H_2O/5% ^2H_2O at 25 °C and pH 6.9. [b] Signal label as in ref *15*.

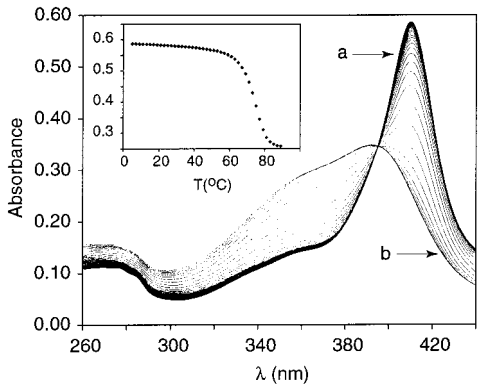

FIGURE 12: Optical spectrum of oxidized S6803 rHb as a function of temperature. The sample was 5.8 μM heme (pH 7.2, 20 mM phosphate). The trace collected at the lowest temperature (5 °C) is indicated with "a" and that at the highest temperature (89 °C) with "b." The inset shows the temperature dependence of the absorbance at 410 nm extracted from these spectra.

(*52*). This geometry is reversed compared to *N. commune* (*53*) Hb and *P. caudatum* Hb (*11*). In *C. eugametos*, the two orientations are equally populated (*11*). The origin and implications of the preference for one isomer over the other are unclear, but the two isomers may differ in properties such as redox potential (*54*).

The CD signal of hemoproteins in the Soret region reflects asymmetric interactions with the residues lining the heme pocket (*55*) and can be used to assess the extent of heme disorder (*56*). Equilibrated ferric S6803 rHb exhibited a negative Cotton effect with a minimum at 407 nm (Figure S3, Supplementary Information) similar to that of wild-type pig and rat hepatic cytochrome b_5 (*57*, *58*).

Thermal Stability of the Hexacoordinated Species. Figure 12 illustrates the results of a thermal denaturation experiment monitoring the holoprotein state by absorption spectroscopy. As the temperature is raised, a smooth transition takes place from the hemichrome spectrum to a spectrum resembling that of free ferric heme. The isosbestic point supports a two-state process by which the protein is either folded and the heme in a hexacoordinate low-spin state or unfolded in the presence of a high-spin heme likely to be loosely and nonspecifically associated with the polypeptide as observed in other thermally unfolded *b* hemoproteins (*59*).

The inset of Figure 12 shows the temperature dependence of the absorbance at 410 nm. The curve reflects the maintenance of the folded state up to 55 °C; this property was confirmed by NMR data up to 45 °C. The thermal

unfolding of the protein at neutral pH was not completely reversible, and the midpoint at 74 °C, obtained with a van't Hoff analysis of the curve (*60*), is only an apparent value. Apparent transition midpoints as high as 77 °C were obtained when the data were collected at a single wavelength to improve the reversibility. Changes in temperature did not trigger a rearrangement of the coordination in the folded state.

Electrochemistry. Experimental evidence thus far supports that the ferrous form of S6803 rHb is also hexacoordinated (*15*) and by the same histidine ligands (*46*). The reduction potential of the Fe(III)/Fe(II) couple was determined in the hexacoordinated S6803 rHb species for comparison to other hemoproteins. The values obtained in two consecutive OSWV scans on two separate samples of S6803 rHb samples in Tris or sodium phosphate buffer yielded a consistent reduction potential value of −150 mV ± 4 mV vs SHE. Samples containing poly-L-lysine in the electrochemical solution at all experimental concentrations returned a potential of −150 mV for the first scan and subsequent readings stabilized at a slightly more positive reduction potential of −139 mV ± 3 mV vs SHE.

DISCUSSION

The elucidation of the relationship between structure and function in hemoglobins requires a complete description of the structural and dynamic features of the heme-binding site. In a step toward understanding the control of reactivity in trHb's, NMR spectroscopy was applied to characterize the ligation scheme and the heme-binding properties of the hexacoordinate hemoglobin from *Synechocystis* sp. PCC 6803. The data demonstrated that, in the wild-type ferric heme-reconstituted S6803 rHb, residues His F8 (His70) and His E10 (His46) coordinate the iron ion. The optical properties of S6803 rHb in the ferrous state are consistent with retention of this hexacoordination scheme (*15*, *46*). Where the identity of the heme ligands is concerned, it can be concluded that S6803 rHb resembles cytochrome b_5.

When comparisons are made to other trHb's, it is noteworthy that the truncated Hb from *N. commune* also contains a histidine at position E10 (*61*) and that this protein does not form a hemichrome as readily as S6803 rHb. Also, in contrast, *C. eugametos* Hb is capable of an unusual lysine E10-assisted coordination of Tyr B10 (*6*) yielding a low-spin complex, but Tyr B10 does not bind the iron in S6803 rHb. In the X-ray structure of the metcyano complex of ferric *C. eugametos* Hb, Lys E10 points away from the heme and the relative disposition of the distal helix and prosthetic group must be perturbed for the side chain to reach the iron. Such a conformational change is plausible since, in *C. eugametos* Hb, Lys E10 becomes the distal ligand when Tyr B10 is replaced by a leucine (*6*). Guertin and colleagues further observed that substitution of His46 in S6803 rHb has no effect on the resonance Raman characteristics of bound carbon monoxide to the reduced heme (*46*). His46 can therefore move away from the exogenous ligand that displaces it.

Endogenous hexacoordination is rare in globins presumably because it interferes with the binding of oxygen. The nonsymbiotic hemoglobin from rice is a recently discovered exception (*62*, *63*) where the distal histidine (E7) ligates the iron in the ferrous state. The kinetics of O_2 binding reflect the displacement of this ligand in a step that is thought to tune the oxygen affinity (*64*, *65*). Conformational changes are triggered by O_2 binding, possibly contributing in a mechanism for signal transduction (*63*). The effects of various exogenous ligands on the structure of S6803 rHb remain to be determined. However, when O_2 is bound, its rate of release appears to be slow (*46*), which suggests that residues such as Tyr B10 and Gln E7 may be recruited to stabilize the complex through the H-bond network (*66*−*68*). Interestingly, the trHb from *P. caudatum* has an unexpectedly low oxygen affinity, although it contains these two H-bonding residues (Figure 1). This has been attributed to conformational equilibria opening the distal side of the protein (*5*) and supports variability in the dynamic properties of trHb heme pockets.

Optical and NMR data indicated that the majority of ferric S6803 rHb molecules lost the heme group with a rate constant comparable to that observed in wild-type sperm whale myoglobin at neutral pH (*42*, *69*) and somewhat lower than that in cytochrome b_5 (*41*). The efficient heme retention in ferric S6803 rHb compared to *N. commune* GlbN is likely to arise in part from the His46−Fe bond. However, the H46A variant of S6803 rHb retains its heme group (*46*), which indicates only a moderate decrease in affinity caused by the replacement. Other factors, for example differences in the sequence bordering the heme (*15*), are therefore likely to contribute strongly to heme affinity in S6803 Hb.

A small fraction of reconstituted S6803 rHb lost the heme faster than the major fraction discussed above. Similar behavior has been reported in other *b* hemoproteins and has been attributed to molecules possessing a detached proximal histidine (*43*). In the present case, the NMR control experiment monitored resolved heme resonances from the major isomer of ferric S6803 rHb, and the fits of the NMR data were improved by the inclusion of a low-amplitude fast phase, as in the optical data. It is doubtful that a change in coordination would be NMR silent over the paramagnetic region of the spectrum, and the nature of this subpopulation is not evident. Support for a minor hemichrome form with subtly different geometry is provided by weak, unattributed cross-peaks in the $^1H-^{15}N$ HSQC data.

As in other *b* hemoproteins, heme reorientation proceeds via a complicated mechanism. The most economical model representing the process calls for eqs 1b and 1c to account for the measurable propensity of the holoprotein to release its heme and for eq 1a as a unimolecular route within a protein cage (*37*). Microscopic reversibility applied to eqs 1a−c holds that $k_1^M k_2^m k_f = k_1^m k_2^M k_b$. If there is no kinetic discrimination for heme insertion, then k_2^m is equal to k_2^M, and it follows that $k_1^m/k_1^M = k_f/k_b$. In S6803 rHb, the equilibrium constant for heme disorder, $K = k_f/k_b = [M]/[m]$, was ∼20 at 25 °C. The rate constant of heme loss from the major isomer, k_1^M, was ∼0.01 h^{-1}, which implied $k_1^m = 0.2$ h^{-1}. The rate constant for intramolecular reorientation, k_f, was estimated at 0.5 h^{-1}. Taking the rate constants at face value, kinetic partitioning could be estimated with simulations that suppressed either the intramolecular or the intermolecular pathway. If heme loss alone were responsible for reorientation, the rate constants indicated that after 1.4 h (approximately 1 half-life) the minor isomer proportion would have decreased from 46% to 40%, whereas if reorientation within the protein were the only mechanism,

25% of the minor isomer would be left. The observed value was 21%, close to the intramolecular prediction.

Three comments should be made about the kinetic simulations. First, the optical data for heme transfer could be modeled with 5% of the total population losing the heme 20 times faster than the major isomer, as proposed above on the basis of the simplest mechanism. This, in effect, resolved eq 2a into eqs 1b and 1c. However, a separate population, as described by eq 2b, remained necessary to fit the data and to account for the biphasic trace observed by NMR spectroscopy. This, as well as the tendency of the hemichrome to produce a species with trapped heme (see Materials and Methods), revealed that sample heterogeneity may interfere with various biophysical measurements. Second, the fit of the NMR data for heme reorientation was satisfactory when two distinct heme insertion rate constants, k_i, were used, k_i^M being ~20% faster than k_i^m. Apparent discrimination in these ad hoc steps could be due to a number of causes, including additional equilibria involving the binding of heme dimers as observed for the insertion of tin protoporphyrin IX in equine apomyoglobin (*70*). This difference in apparent rate constants does not necessarily invalidate the assumption that $k_2^M = k_2^m$. Third, all rate constants obtained on this system were approximate because several assumptions were necessary to fit the data and some of the processes occurred on similar time scales. The most accurate parameter that could be extracted from the experiments was the intramolecular rate constant, k_f.

In myoglobin, an intramolecular mechanism of heme reorientation (eq 1a) is supported by the negative results of heme displacement experiments (*37*). The rate of heme reorientation in S6803 rHb at 25 °C is approximately 35 times faster than that reported for sperm whale Mb in the metaquo form ($k_f \sim 4 \times 10^{-6}$ s^{-1}, at pH 7.2; *37*) and 10 times faster than for cytochrome b_5 (*71*). The similar activation energies for reorientation of m into M in sperm whale metaquoMb (*72*), heme dissociation from the protein matrix (*43*), and heme reorientation in S6803 rHb (this work) suggest that the processes occur with conserved mechanistic features: breaking of axial bond(s), local unfolding, and solvation of the heme group. An interpretation of the common behavior proposes that decoordination of His46 in S6803 rHb plays no part in the rate-limiting step of either heme loss or heme reorientation. This would support a relatively weak His46−Fe bond, as suspected from the H46A variant data (*46*); this is an advantage if the function of the protein is to bind an exogenous ligand in the distal cavity.

The stability of ferric S6803 rHb toward thermal denaturation at neutral pH compares well with the stability of sperm whale myoglobin (*73*) and cytochrome b_5 (*74*) if the apparent T_m is used as an indicator of the robustness of the protein. According to CD data, the extent of secondary structure induced by heme binding to S6803 apoHb is approximately 30%. On a residue basis, such an increase is comparable to that in sperm whale myoglobin (*75*). Quantitative interpretation of CD data is unreliable for apoglobins (*76*, *77*); nevertheless, it is expected that a fraction of the binding Gibbs energy is expended in the refolding of the truncated sequence. Coupled binding−refolding as observed here is typical of *b* hemoproteins with buried prosthetic groups (*78*).

The standard reduction potential of the iron ion in hemoproteins depends on numerous influences including coordination scheme (*79*, *80*), exposure of the heme group to solvent (*81*), H-bonding status (*82*) and orientation (*83*) of axial ligands, and dielectric properties of the heme pocket (*84*). The midpoint potential of S6803 rHb between pH 7 and pH 8 was measured to be ~−150 mV vs SHE with and without poly-L-lysine; this value is more negative than typically encountered in globins and b_5 cytochromes (*54*, *85*, *86*). It is likely that bishistidine coordination contributes to the low potential as proposed for V68H horse myoglobin (*83*). This protein, in which His68 (E11) binds the iron, has a midpoint potential of −110 mV vs SHE, some 170 mV lower than wild-type horse myoglobin.

The p*I* of S6803 rHb is below neutral, and the sequence alignment with *C. eugametos* Hb shows that several acidic residues border the heme cavity. These two features are shared with cytochrome b_5 where they are thought to contribute to unique electrochemical properties, including a midpoint potential sensitive to mediators. Key to the unusual electrochemistry of cytochrome b_5 is also a heme group with one edge exposed to solvent (*87*). Whether S6803 rHb exhibits similar modulation of electrochemical properties will be established with further potential determinations.

In myoglobins a serine is generally found at the position preceding the proximal histidine. This side chain forms an H-bond with the proximal histidine and orients the imidazole ring (*88*, *89*), increases its imidazolate character, and stabilizes the oxidized state. Removal of this interaction increases the affinity for distal ligands (*90*, *91*). In S6803 rHb, both His46 and His70 are preceded by an alanine incapable of side-chain H-bonding interactions. The moderate shifts of the Cβ*H*'s of the axial histidines (Table 1) also suggest that H-bonding to the NδH's does not take place (*32*). For example, in peroxidases Cβ*H*'s are found between 14 and 22 ppm (*32*); in cytochrome b_5, one of the CβH's of axial His39, whose NδH forms a strong hydrogen bond to the carbonyl of Gly42, resonates at 16 ppm, whereas the CβH's of axial His63, whose NδH forms a weak hydrogen bond to the carbonyl of Phe58, resonate near 10 ppm (*36*, *92*). Low imidazolate character, if confirmed, could provide one explanation for the stabilization of endogenous hexacoordination.

In conclusion, essential features of the heme-binding site of trHb from *Synechocystis* sp. PCC 6803 were inspected. It was found that the protein retains the heme efficiently within its cavity, selects preferentially one of the heme positional isomers, and has a negative standard reduction potential. The reversible formation of a bishistidyl heme complex accounts for some of these properties. As in rice Hb, the interactions of the heme with the two axial histidines are not equivalent, and the distal residue can be displaced by an exogenous ligand. In addition, the observation of a small population of hexacoordinate globin in the S6803 H46A variant (*46*) shows that this protein is capable of ligand exchange and conformational rearrangements. Ligand exchange and displacement reactions provide a versatile means to control the functional properties of a hemoprotein. Such processes take place not only in hexacoordinate globins but also in several other hemoproteins, for example, the translational activator CooA (*93*) and the hemophore HasA (*94*). The bishistidyl scheme encountered in S6803 Hb raises

questions about the role of the protein in vivo and offers an opportunity to investigate novel globin chemistry. A detailed description of the heme environment and the hydrogen bond network involving the axial residues will be crucial in the rationalization of the redox and ligand-binding properties of this protein and its relatives.

ACKNOWLEDGMENT

The authors thank Dr. C. R. Matthews for continuous support, Dr. D. A. Bryant for numerous discussions, Dr. A. D. Jones for the collection of mass spectrometry data, and Dr. J. H. Golbeck for the use of the electrochemical equipment. Dr. J. A. Zitzewitz provided assistance in the collection of CD data. The Voyager mass spectrometer (Penn State Intercollegiate Center for Mass Spectrometry) and the Bruker DRX-600 NMR spectrometer were purchased in part with funds from the National Institutes of Health, Grants S10 RR11318 and S10 RR10524, respectively; the BAS 100B electrochemical analyzer was purchased in part with funds from the National Science Foundation (Award 9602232). Figure 2A was generated with MOLSCRIPT (*95*).

SUPPORTING INFORMATION AVAILABLE

Protocols for protein purification and heme titration and figures of (1) the titration of apo S6803 rHb with hemin, (2) the $^{1}H-^{15}N$ HSQC of ferric S6803 rHb, (3) the Soret CD spectrum of ferric S6803 rHb, and (4) heme loss from ferric S6803 rHb. This material is available free of charge via the Internet at http://pubs.acs.org.

REFERENCES

1. Couture, M., Chamberland, H., St-Pierre, B., Lafontaine, J., and Guertin, M. (1994) *Mol. Gen. Genet. 243*, 185−197.
2. Iwaasa, H., Takagi, T., and Shikama, K. (1990) *J. Biol. Chem. 265*, 8603−8609.
3. Iwaasa, H., Takagi, T., and Shikama, K. (1989) *J. Mol. Biol. 208*, 355−358.
4. Hill, D. R., Belbin, T. J., Thorsteinsson, M. V., Bassam, D., Brass, S., Ernst, A., Boger, P., Paerl, H., Mulligan, M. E., and Potts, M. (1996) *J. Bacteriol. 178*, 6587−6598.
5. Das, T. K., Weber, R. E., Dewilde, S., Wittenberg, J. B., Wittenberg, B. A., Yamauchi, K., Van Hauwaert, M. L., Moens, L., and Rousseau, D. L. (2000) *Biochemistry 39*, 14330−14340.
6. Das, T. K., Couture, M., Lee, H. C., Peisach, J., Rousseau, D. L., Wittenberg, B. A., Wittenberg, J. B., and Guertin, M. (1999) *Biochemistry 38*, 15360−15368.
7. Couture, M., Yeh, S. R., Wittenberg, B. A., Wittenberg, J. B., Ouellet, Y., Rousseau, D. L., and Guertin, M. (1999) *Proc. Natl. Acad. Sci. U.S.A. 96*, 11223−11228.
8. Springer, B. A., Sligar, S. G., Olson, J. S., and Philips, G. N. J. (1994) *Chem. Rev. 94*, 699−714.
9. Ptitsyn, O. B., and Ting, K. L. (1999) *J. Mol. Biol. 291*, 671−682.
10. Perutz, M. F., Wilkinson, A. J., Paoli, M., and Dodson, G. G. (1998) *Annu. Rev. Biophys. Biomol. Struct. 27*, 1−34.
11. Pesce, A., Couture, M., Dewilde, S., Guertin, M., Yamauchi, K., Ascenzi, P., Moens, L., and Bolognesi, M. (2000) *EMBO J. 19*, 2424−2434.
12. Tsubamoto, Y., Matsuoka, A., Yusa, K., and Shikama, K. (1990) *Eur. J. Biochem. 193*, 55−59.
13. Thorsteinsson, M. V., Bevan, D. R., Ebel, R. E., Weber, R. E., and Potts, M. (1996) *Biochim. Biophys. Acta 1292*, 133−139.
14. Couture, M., Das, T. K., Lee, H. C., Peisach, J., Rousseau, D. L., Wittenberg, B. A., Wittenberg, J. B., and Guertin, M. (1999) *J. Biol. Chem. 274*, 6898−6910.
15. Scott, N. L., and Lecomte, J. T. J. (2000) *Protein Sci. 9*, 587−597.
16. Gill, S. C., and von Hippel, P. H. (1989) *Anal. Biochem. 182*, 319−326.
17. Antonini, E., and Brunori, M. (1971) *Hemoglobin and myoglobin in their reactions with ligands*, Vol. 12, North-Holland, Amsterdam.
18. de Duve, C. (1948) *Acta Chem. Scand. 2*, 264−289.
19. Falzone, C. J., Mayer, M. R., Whiteman, E. L., Moore, C. D., and Lecomte, J. T. J. (1996) *Biochemistry 35*, 6519−6526.
20. Schmid, F. X. (1989) in *Protein structure. A practical approach* (Creighton, T. E., Ed.) pp 251−285, IRL Press, New York.
21. Live, D. H., Davis, D. G., Agosta, W. C., and Cowburn, D. (1984) *J. Am. Chem. Soc. 106*, 1939−1941.
22. Kay, L. E., Xu, G.-Y., Singer, A. U., Muhandiram, D. R., and Forman-Kay, J. D. (1993) *J. Magn. Reson., Ser. B 101*, 333−337.
23. Muhandiram, D. R., Farrow, N. A., Xu, G.-Y., Smallcombe, S. H., and Kay, L. E. (1993) *J. Magn. Reson., Ser. B 102*, 317−321.
24. Kay, L. E., Ikura, M., Tschudin, R., and Bax, A. (1990) *J. Magn. Reson. 89*, 496−514.
25. Bax, A., and Ikura, M. (1991) *J. Biomol. NMR 1*, 99−104.
26. Grzesiek, S., and Bax, A. (1992) *J. Magn. Reson. 99*, 201−207.
27. Cavanagh, J., Fairbrother, W. J., Palmer, A. G. I., and Skelton, N. J. (1996) *Protein NMR Spectroscopy. Principles and Practice*, Academic Press, San Diego, CA.
28. Marion, D., Ikura, M., Tschudin, R., and Bax, A. (1989) *J. Magn. Reson. 85*, 393−399.
29. Piotto, M., Saudek, V., and Sklenář, V. (1992) *J. Biomol. NMR 2*, 661−665.
30. Sklenář, V., Piotto, M., Leppik, R., and Saudek, V. (1993) *J. Magn. Reson. 102*, 241−245.
31. Inubushi, T., and Becker, E. D. (1983) *J. Magn. Reson. 51*, 128−133.
32. La Mar, G. N., Satterlee, J. D., and de Ropp, J. S. (2000) in *The Porphyrins Handbook* (Smith, K. M., Kadish, K., and Guilard, R., Eds.) pp 185−298, Academic Press, Burlington, MA.
33. Lyons, T. A., Ratnaswamy, G., and Pochapsky, T. C. (1996) *Protein Sci. 5*, 627−639.
34. Unger, S. W., Jue, T., and La Mar, G. N. (1985) *J. Magn. Reson. 61*, 448−456.
35. Nguyen, B. D., Xia, Z., Yeh, D. C., Vyas, K., Deaguero, H., and La Mar, G. N. (1999) *J. Am. Chem. Soc. 121*, 208−217.
36. McLachlan, S. J., La Mar, G. N., and Lee, K. B. (1988) *Biochim. Biophys. Acta 957*, 430−445.
37. La Mar, G. N., Toi, H., and Krishnamoorthi, R. (1984) *J. Am. Chem. Soc. 106*, 6395−6401.
38. Barshop, B. A., Wrenn, R. F., and Frieden, C. (1983) *Anal. Biochem. 130*, 134−145.
39. Dang, Q., and Frieden, C. (1997) *Trends Biochem. Sci. 22*, 317.
40. Hargrove, M. S., Barrick, D., and Olson, J. S. (1996) *Biochemistry 35*, 11293−11299.
41. Hunter, C. L., Lloyd, E., Eltis, L. D., Rafferty, S. P., Lee, H., Smith, M., and Mauk, A. G. (1997) *Biochemistry 36*, 1010−1017.
42. Liong, E. C., Dou, Y., Scott, E. E., Olson, J. S., and Phillips, G. N., Jr. (2001) *J. Biol. Chem. 276*, 9093−9100.
43. Smith, M. L., Paul, J., Ohlsson, P. I., Hjortsberg, K., and Paul, K. G. (1991) *Proc. Natl. Acad. Sci. U.S.A. 88*, 882−886.
44. Teale, F. W. J. (1959) *Biochim. Biophys. Acta 35*, 543.
45. Osteryoung, J. (1988) *Methods Enzymol. 158*, 243−267.
46. Couture, M., Das, T. K., Savard, P. Y., Ouellet, Y., Wittenberg, J. B., Wittenberg, B. A., Rousseau, D. L., and Guertin, M. (2000) *Eur. J. Biochem. 267*, 4770−4780.
47. Dangi, B., Sarma, S., Yan, C., Banville, D. L., and Guiles, R. D. (1998) *Biochemistry 37*, 8289−8302.
48. Banci, L., Bertini, I., Rosato, A., and Scacchieri, S. (2000) *Eur. J. Biochem. 267*, 755−766.

49. Sukits, S. F., and Satterlee, J. D. (1996) *Biophys. J. 71*, 2848−2856.
50. La Mar, G. N., Burns, P. D., Jackson, J. T., Smith, K. M., Langry, K. C., and Strittmatter, P. (1981) *J. Biol. Chem. 256*, 6075−6079.
51. Kuzelova, K., Mrhalova, M., and Hrkal, Z. (1997) *Biochim. Biophys. Acta 1336*, 497−501.
52. Emerson, S. D., and La Mar, G. N. (1990) *Biochemistry 29*, 1556−1566.
53. Yeh, D. C., Thorsteinsson, M. V., Bevan, D. R., Potts, M., and La Mar, G. N. (2000) *Biochemistry 39*, 1389−1399.
54. Walker, F. A., Emrick, D., Rivera, J. E., Hanquet, B. J., and Buttlaire, D. H. (1988) *J. Am. Chem. Soc. 110*, 6234−6340.
55. Hsu, M. C., and Woody, R. W. (1971) *J. Am. Chem. Soc. 93*, 3515−3525.
56. Aojula, H. S., Wilson, M. T., Moore, G. R., and Williamson, D. J. (1988) *Biochem. J. 250*, 853−858.
57. Schnellbacher, E., and Lumper, L. (1971) *Hoppe-Seyler's Z. Physiol. Chem. 352*, 615−628.
58. Ihara, M., Takahashi, S., Ishimori, K., and Morishima, I. (2000) *Biochemistry 39*, 5961−5970.
59. Robinson, C. R., Liu, Y., O'Brien, R., Sligar, S. G., and Sturtevant, J. M. (1998) *Protein Sci. 7*, 961−965.
60. Dill, K. (1990) *Biochemistry 29*, 7133−7155.
61. Potts, M., Angeloni, S. V., Ebel, R. E., and Bassam, D. (1992) *Science 256*, 1690−1691.
62. Arredondo-Peter, R., Hargrove, M. S., Sarath, G., Moran, J. F., Lohrman, J., Olson, J. S., and Klucas, R. V. (1997) *Plant Physiol. 115*, 1259−1266.
63. Hargrove, M. S., Brucker, E. A., Stec, B., Sarath, G., Arredondo-Peter, R., Klucas, R. V., Olson, J. S., and Phillips, G. N. (2000) *Struct. Fold. Des. 8*, 1005−1014.
64. Hargrove, M. S. (2000) *Biophys. J. 79*, 2733−2738.
65. Trent, J. T., Hvitved, A., and Hargrove, M. S. (2001) *Biochemistry* (in press).
66. Kloek, A. P., Yang, J., Mathews, F. S., Frieden, C., and Goldberg, D. E. (1994) *J. Biol. Chem. 269*, 2377−2379.
67. De Baere, I., Perutz, M. F., Kiger, L., Marden, M. C., and Poyart, C. (1994) *Proc. Natl. Acad. Sci. U.S.A. 91*, 1594−1597.
68. Miele, A. E., Santanche, S., Travaglini-Allocatelli, C., Vallone, B., Brunori, M., and Bellelli, A. (1999) *J. Mol. Biol. 290*, 515−524.
69. Hargrove, M. S., Wilkinson, A. J., and Olson, J. S. (1996) *Biochemistry 35*, 11300−11309.
70. Deeb, R. S., and Peyton, D. H. (1992) *Biochemistry 31*, 468−474.
71. Singh, H. K., and Wilson, M. T. (1990) *Biochem. Soc. Trans. 18*, 1272−1273.
72. Yee, S., and Peyton, D. H. (1995) *Biochim. Biophys. Acta 1252*, 295−299.
73. Privalov, P. L., Griko, Y. V., Venyaminov, S. Y., and Kutyshenko, V. P. (1986) *J. Mol. Biol. 190*, 487−498.
74. Pfeil, W. (1993) *Protein Sci. 2*, 1497−1501.
75. Breslow, E., Beychok, S., Hardman, K. D., and Gurd, F. R. N. (1965) *J. Biol. Chem. 240*, 304−309.
76. Hughson, F. M., Wright, P. E., and Baldwin, R. L. (1990) *Science 249*, 1544−1548.
77. Lecomte, J. T. J., Kao, Y.-H., and Cocco, M. J. (1996) *Proteins: Struct., Funct., Genet. 25*, 267−285.
78. Falzone, C. J., Wang, Y., Vu, B. C., Scott, N. L., Bhattacharya, S., and Lecomte, J. T. J. (2001) *Biochemistry 40*, 4879−4891.
79. Moore, G. R., and Pettigrew, G. W. (1990) in *Cytochromes c. Evolutionary, structural and physicochemical aspects* (Rich, A., Ed.) Springer-Verlag, New York.
80. Tezcan, F. A., Winkler, J. R., and Gray, H. B. (1998) *J. Am. Chem. Soc. 120*, 13383−13388.
81. Stellwagen, E. (1978) *Nature 275*, 73−74.
82. Goodin, D. B., and McRee, D. E. (1993) *Biochemistry 32*, 3313−3324.
83. Lloyd, E., Hildebrand, D. P., Tu, K. M., and Mauk, A. G. (1995) *J. Am. Chem. Soc. 117*, 6434−6438.
84. Kassner, R. J. (1972) *Proc. Natl. Acad. Sci. U.S.A. 69*, 2263−2267.
85. Lee, K. B., Jun, E., La Mar, G. N., Rezzano, I. N., Pandey, R. K., Smith, K. M., Walker, F. A., and Buttlaire, D. H. (1991) *J. Am. Chem. Soc. 113*, 3576−3583.
86. Wang, Z. Q., Wang, Y. H., Wang, W. H., Xue, L. L., Wu, X. Z., Xie, Y., and Huang, Z. X. (2000) *Biophys. Chem. 83*, 3−17.
87. Rivera, M., Seetharaman, R., Girdhar, D., Wirtz, M., Zhang, X., Wang, X., and White, S. (1998) *Biochemistry 37*, 1485−1494.
88. Peterson, E. S., Friedman, J. M., Chien, E. Y., and Sligar, S. G. (1998) *Biochemistry 37*, 12301−12319.
89. Wu, Y., Chien, E. Y., Sligar, S. G., and La Mar, G. N. (1998) *Biochemistry 37*, 6979−6990.
90. Smerdon, S. J., Krzywda, S., Wilkinson, A. J., Brantley, R. E., Jr., Carver, T. E., Hargrove, M. S., and Olson, J. S. (1993) *Biochemistry 32*, 5132−5138.
91. Barrick, D. (2000) *Proteins 39*, 291−308.
92. Lee, K. B., McLachlan, S. J., and La Mar, G. N. (1994) *Biochim. Biophys. Acta 1208*, 22−30.
93. Aono, S., Honma, Y., Ohkubo, K., Tawara, T., Kamiya, T., and Nakajima, H. (2000) *J. Inorg. Biochem. 82*, 51−56.
94. Arnoux, P., Haser, R., Izadi, N., Lecroisey, A., Delepierre, M., Wandersman, C., and Czjzek, M. (1999) *Nat. Struct. Biol. 6*, 516−520.
95. Kraulis, P. (1991) *J. Appl. Crystallogr. 24*, 946−950.

BI010226U